

Cite this: *Mater. Adv.*, 2026,
7, 3518Received 9th February 2026,
Accepted 18th March 2026

DOI: 10.1039/d6ma00185h

rsc.li/materials-advances

How well do conventional atomistic simulations predict adsorption binding sites in metal–organic frameworks compared to experiment?

Jake Burner,[†] Olivier Marchand,[†] Sari Warshawsky, Marco Gibaldi[†] and Tom K. Woo^{*}

Classical force fields are widely used for simulating adsorption in MOFs, and limitations for global properties such as uptakes are known. For the first time, experimental binding sites across diverse MOFs and adsorbates were compared against simulated results to demonstrate that classical force fields reliably reproduce binding site locations even when adsorption isotherms disagree. Errors arising from experimental uncertainty and approximations of routine classical simulations such as flexibility and chemisorption are evaluated.

Gas separation and storage is one of the most widely studied applications of metal–organic framework (MOF) materials, where it is reaching commercialization. For example, CALF-20¹ is being scaled for industrial CO₂ capture from cement-manufacturing flues,² and MOFs are being deployed for safe storage and transport of toxic gases.^{3,4} Central to these applications are the adsorption binding sites (ABSs), which govern affinity and selectivity and therefore play a fundamental role in applications from gas storage and separation⁵ to catalysis and sensing.⁶ Although >100 000 MOFs have been experimentally characterized and deposited in the CSD,^{7,8} direct observation of adsorbates in these materials using crystallography is relatively rare, often requiring synchrotron radiation sources.^{9,10} While other techniques are often used to probe adsorbate interactions in MOFs (e.g., NMR), these usually rely on other experimental or computational methods to elucidate the detailed positions of adsorbates.^{11,12}

Atomistic grand canonical Monte Carlo (GCMC) simulations have become a common tool for modelling gas adsorption in MOFs and other porous materials.^{13,14} GCMC is particularly popular for simulating gas adsorption isotherms of MOFs. The simulation method can be characterized as a brute-force technique where interaction energies are computed for millions of

configurations to generate a single isotherm point using the machinery of statistical mechanics. Therefore, practical use of GCMC simulations generally relies on simplified approximations, which limit their accuracy. For example, generic force field parameters (e.g., UFF¹⁵) are used to compute pairwise Lennard-Jones potentials to model steric/dispersion interactions, while fixed partial atomic charges are used to model electrostatic interactions (obtained either from empirical models,¹⁶ ML models,¹⁷ or fit to DFT potentials^{18,19}). In addition to these approximations, the MOF is often modelled as a rigid, defect-free crystal.

The accuracy of these approximations and sensitivity to adsorption properties such as uptakes and diffusion of MOFs have been extensively studied.^{14,20,21} For example, Cleeton *et al.*¹⁴ and McCready *et al.*²⁰ conducted large systematic evaluations of classical GCMC simulations for computing CO₂ isotherms in MOFs, and both reported significant variability in predicted uptake, especially when open metal sites (OMSs) are present. Goeminne *et al.*²² showed that even small interaction energy errors (~ 4 kJ mol⁻¹) and subtle framework distortions can strongly impact predicted isotherms. Together, these results indicate that common GCMC approximations may be insufficient for reliable isotherm prediction *versus* experiment. However, while such limitations are known for global observables, their effect on local properties like experimentally resolved ABSs remains much less understood.

In this work, we address this gap by curating a crystallography dataset of directly observed adsorbate positions spanning 23 MOFs with varying degrees of accessible OMSs, flexibility, and dimensionality and eight adsorbates (CO₂, C₂H₂, CH₄, NO, Ar, Xe, Kr, and H₂O). The set was restricted to structures where the adsorbate and MOF atomic positions were fully defined from crystallography. Structures with highly disordered sites or those which relied on computational refinement (e.g., DFT calculations) were excluded since optimized geometries from DFT calculations typically correspond to minima on the single-guest potential energy surface that

Department of Chemistry and Biomolecular Sciences, University of Ottawa,
10 Marie Curie Pvt, Ottawa, K1N 6N5, Canada. E-mail: tom.woo@uottawa.ca

[†] These authors contributed equally to this work.



Table 1 List of MOF/adsorbate/condition combinations (MACs) where detailed guest positions have been determined experimentally, the conditions they were acquired, and a comparison of the experimental and GCMC determined binding sites

MOF name	OMS ^a	flexibility ^b	No.	Guest	T (K)	P (bar)	Cryst. (R-factor)	RMSD _{COM} ^c	RMSD/atom ^d	Ref.
[Rh ₂ (bza) ₄ (dimethyl-pyz)] _n	No	Slight increase in volume at high loading	1	CO ₂	90	1	SCXRD (0.047)	0.153	0.263	23
			2	CO ₂	90	17	SCXRD (0.103)	0.199	0.205	23
CALF-20	No	Slight phase change with water adsorption	3	CO ₂	296	10	SCXRD (0.030)	0.156	0.221	24
			4	H ₂ O	296	—	PXRD (0.0418)	1.026	1.026	25
Mg(HCOO) ₂	No	—	5	C ₂ H ₂	90	—	SCXRD (0.040)	0.770	0.854	26
Mn(HCOO) ₂	No	—	6	C ₂ H ₂	90	—	SCXRD (0.034)	0.788	0.867	26
CALF-15	No	—	7	CO ₂	173	0.85	SCXRD (0.030)	0.262	0.323	27
Sc ₂ (BDC) ₃	No	Slight rotational freedom of BDC linkers	8	CH ₄	230	9	SCXRD (0.040)	0.231	0.231	28
			9	CO ₂	235	1	SCXRD (0.071)	0.273	0.283	28
MUF-16(Mn)	No	—	10	CO ₂	293	1.1	SCXRD (0.051)	1.283	1.446	29
MOF-74(Ni) (capped ^f)	No	—	11	NO	300	0.08	SCXRD (0.049)	—	—	30
SBMOF-1	No	—	12	Xe	100	—	SCXRD (0.084)	0.256	0.256	31
			13	Kr	100	—	SCXRD (0.052)	0.180	0.180	31
[Rh ₂ (bza) ₄ (pyz)] _n	No	Guest-induced phase change	14	Ar	298	80	SCXRD (0.115)	0.243	0.243	32
			15	CO ₂	298	35	SCXRD (0.105)	0.169	0.389	32
			16	CO ₂	93	1.01	SCXRD (0.103)	0.208	0.231	33
[Cu ₂ (bza) ₄ (pyz)] _n	No	Guest-induced phase change	17	CO ₂	193	1.01	SCXRD (0.147)	0.196	0.207	34
[Rh ₂ (bza) ₄ (2-epyz)] _n	No	Guest-induced phase change	18	CO ₂	298	64	SCXRD (0.077)	0.145	0.397	35
			19	CO ₂	90	36	SCXRD (0.168)	0.174	0.192	35
NH ₂ -MIL-53(Al)	No	Various phases of pore opening	20	CO ₂	253	3.0	PXRD (—)	0.950	1.331	36
			21	CO ₂	253	9.5	PXRD (—)	1.395	1.499	36
			22	CO ₂	253	18	PXRD (—)	0.607	1.062	36
CPL-1	Yes	—	23	C ₂ H ₂	170	0.1	PXRD (0.320)	0.123	0.159	37
INAIP-Cu	Yes	—	24	C ₂ H ₂	110	0.18	SCXRD (0.041)	0.634	1.026	38
			25	C ₂ H ₂	153	0.85	SCXRD (0.036)	0.660	0.708	38
MOF-74(Co)	Yes	—	26	CO ₂	10	—	NPD (0.029)	0.393	0.481	39 ^e
			27	NO	298	1.01	PXRD (0.058)	1.148	1.679	40
MOF-74(Fe)	Yes	—	28	CO ₂	298	1	NPD (0.018)	0.550	0.738	39 ^e
MOF-74(Mg)	Yes	—	29	CO ₂	10	—	NPD (0.022)	0.659	0.776	39 ^e
MOF-74(Zn)	Yes	—	30	CO ₂	10	—	NPD (0.031)	0.456	0.642	39 ^e
MOF-74(Ni)	Yes	—	31	NO	300	0.4	SCXRD (0.055)	1.323	1.495	30
[Cu ₂ (pyrdc) ₂ (bpp) ₂] _n	Yes	Pillared bilayer; guest-induced phase change	32	CO ₂	193	—	PXRD (0.059)	0.460	0.483	41
MAF-2(Zn)	Yes	Possible guest-induced flexibility; rotational freedom of ethyl groups	33	C ₂ H ₂	195	10.1	SCXRD (0.039)	0.177	0.545	42
			34	CO ₂	195	20.3	SCXRD (0.046)	0.212	0.316	42
MAF-23(Zn)	Yes	Guest-induced flexibility at binding site	35	CO ₂	195	0.79	SCXRD (0.039)	0.998	1.547	43

^a MOF contains open metal site (OMS). ^b Notes on any mention of flexibility in the cited publication(s). ^c RMSD (Å) between experimental and GCMC centres of mass of binding sites. ^d RMSD per atom (Å) between GCMC and experimental binding site coordinates. ^e In the MOF-74 study from Queen *et al.*, both NPD and SC-XRD studies were performed and were in agreement. ^f Secondary site observed when some OMSs were capped by water; disorder/missing protons prevented direct RMSD comparison.

neglects guest-guest interactions, thermal, and entropic effects. An exhaustive search of the literature resulted in a total of 35 MOF/adsorbate/condition combinations (MACs), for which “conventional” GCMC simulations were performed to obtain atom-specific adsorbate probability distributions (APDs). The maxima of the APDs correspond to free-energy minima, known as the adsorption binding sites (ABSs). We define a simulation as being “conventional” if the following approximations are used: (a) the framework is assumed to be rigid and defect-free; (b) generic classical force fields are used for the MOF framework to model dispersion interactions; and (c) fixed partial charges are used to model electrostatics (*i.e.*, polarization is neglected). The ABSs were fit to the APDs using our in-house code GALP (manuscript in preparation; see SI for details). Each of the 35 MACs were assigned an ID given in Table 1, column 4. There are many examples of ABSs of 1D M(II) benzoate pyrazines in the literature, of which we have selected four (**14–16** = Rh(II), **17** = Cu(II), **18–19** = Rh(II) with

2-ethylpyrazine, **1–2** = Rh(II) with dimethylpyrazine) to prevent redundancy (the variants possess similar ABSs). Two examples of M(II) formates (**5** = Mg(II) and **6** = Mn(II)) were also included. CALF-15 (**7**) and CALF-20 (**3–4**) are both Zn(II) MOFs composed of oxalate and triazolate linkers, differing only by amine functionalization. Finally, the MOF-74 analogues studied in this work (**11**, **26–31**) only differ by metal centre identity and/or degree of OMS capping. This results in 12 classes of structures that exhibit notably unique geometries and chemical compositions.

Fig. 1 compares experimentally determined ABSs with those obtained from GCMC simulations for representative MACs (full set shown in Fig. S3–38). These figures show that the general positions of the experimental ABSs are well reproduced by the GCMC simulations in almost all cases. The centre-of-mass RMSD between the computed and experimental ABSs (Table 1) is only 0.51 Å averaged over all MACs. This is excellent overall agreement considering this corresponds to only a few



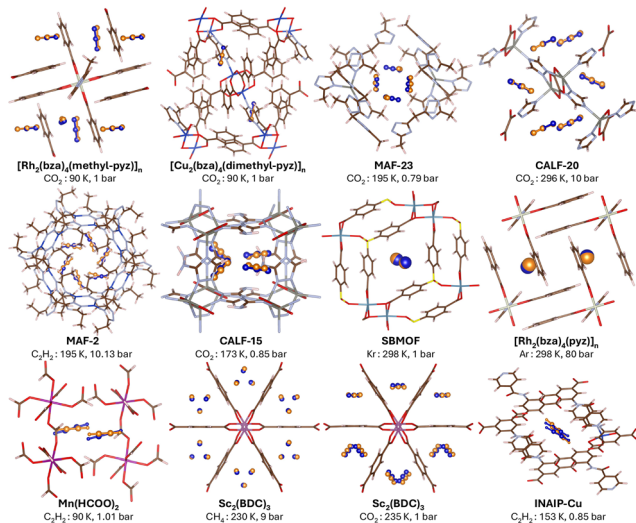


Fig. 1 Comparison of ABS positions obtained from GCMC simulations (blue balls) and from crystallography experiments (orange balls) for a variety of MOFs and adsorbates selected from Table 1. Each MOF is labelled with the guest, temperature and pressure at which the crystallography and GCMC simulations were performed. Importantly, ABSs correspond to free energy minima instead of potential energy minima.

grid points on the 0.15 Å resolution APD grids. The standard deviation is $\sim 75\%$ of the mean, highlighting the presence of several outliers, which are discussed in more detail below. In addition to reproducing general ABS positions, the correct number of sites match experiment in all cases except MAC 32 ($[\text{Cu}_2(\text{pyrdc})_2(\text{bpp})_2]_n$), where GCMC predicts one additional CO_2 per asymmetric unit that is $\sim 25\text{--}35\%$ weaker than the others. Experimental and simulated saturation uptakes are internally consistent with full occupation of their respective ABSs (*i.e.*, GCMC predicts higher saturation uptake because it includes an extra site, and *vice versa* for experiment). The discrepancy therefore likely reflects incomplete activation and/or uncertainty in the refined structure.

For polyatomic adsorbates, the RMSD per atom was computed to incorporate adsorbate orientation in comparing simulated and experimental ABSs. Across all MACs, the mean RMSD/atom is 0.66 Å, well below the ~ 2 Å threshold commonly considered a good fit in molecular docking studies.⁴⁴ This agreement is achieved despite using rigid adsorbates whose fixed internal geometries can differ from crystallography (*e.g.*, the bond length of NO in MAC 27 is unusually long experimentally at 1.43 Å *vs.* 1.15 Å from the molecular force field). Such mismatches contribute an average residual RMSD of 0.06 Å ($\sim 10\%$ of the mean).

Classical, rigid GCMC simulations should perform worst when the approximations are most severe, most notably when MOFs present significant framework flexibility and open metal sites (OMSs), since in such cases generalized force fields are insufficient. To investigate this hypothesis, we group the 35 MACs into four categories: (i) no OMSs/minimal flexibility (MACs 1–13); (ii) no OMSs/significant flexibility (MACs 14–22); (iii) OMSs/no flexibility (MACs 23–31); and (iv) OMSs/significant

flexibility (MACs 32–35). As expected, category (i) MACs show the best agreement (mean RMSD/atom = 0.47 Å, *vs.* 0.66 Å overall), whereas category (iv) is worse (0.72 Å). Category (ii) (14–22) is intermediate (0.62 Å), although most “flexibility” here reflects abrupt phase transitions (except $\text{NH}_2\text{-MIL-53(Al)}$), limiting broader conclusions. Interestingly, MACs from category (iii) (23–31) have the largest mean RMSD/atom of 0.86 Å. While unexpected, this is due to the fact that category (iii) MACs contain two cases in which the adsorbate (NO) binds chemisorptively and the GCMC simulations invert the binding mode (*vide infra*) giving rise to large RMSDs. Furthermore, the OMSs in category (iv) are not nearly as accessible to the adsorbates as MOF-74, which makes up the bulk of MACs in category (iii).

A perhaps surprising observation is that qualitatively poor agreement in the adsorption isotherms, a global adsorption property, does not necessarily preclude accurate ABS identification, a local property. Fig. S3–S8 show the adsorption isotherm comparisons—of available isotherms, about half were performed at the same temperature as the crystallography experiments. The experimental and simulated isotherms typically share the same shape, but differ in steepness (*e.g.*, MAF-2, CALF-15, SBMOF-1, the M(II) formates, and the MOF-74 series). For example, MOF-74(Co)@ CO_2 (26) shows a nearly linear simulated isotherm *versus* a much steeper experimental one (Fig. 2a), yet the ABSs agree well (RMSD = 0.48 Å). This reflects that ABS positions are governed by *relative* interaction energies (positions of free-energy minima), whereas uptake and isotherm steepness depend on *absolute* adsorption energetics (depth of minima). Considering the exponential dependence of occupancies on energies, even modest energetic errors (~ 4 kJ mol⁻¹ (ref. 22)) can strongly affect uptake/coverage while leaving site positions largely unchanged. Moreover, MOF-74 ABS positions remain accurate across metals even when isotherms deviate. Corroborating this, the degree of isotherm agreement correlates directly with the agreement in isosteric heats of adsorption (Table S1).

Differences in isotherm shape (*e.g.*, CPL-1, the M(II) benzoate pyrazines, and $\text{NH}_2\text{-MIL-53(Al)}$) often arise because these MOFs are flexible and undergo guest-induced phase transitions, so rigid-framework simulations are not expected to reproduce the full pressure range; nevertheless, the simulated ABSs are typically still in good agreement with experiment when the correct phase is modelled. A clear example is $[\text{Rh}_2(\text{bza})_4(2\text{-epyz})]_n @ \text{CO}_2$ (18–19), which shows an abrupt α to β transition that appears near 0.28 bar in the experimental isotherm (Fig. 2c(i)); using the fixed structure of each phase at the appropriate pressure yields good agreement for both isotherms and ABSs. By contrast, $\text{NH}_2\text{-MIL-53(Al)}$ shows qualitatively different simulated *vs.* experimental CO_2 sites across three phases (Fig. S21), but here the experimental sites come from *in situ* PXRD/Rietveld refinement and the original authors report peak evidence for phase coexistence at intermediate pressures. This in conjunction with the fact that such procedures do not necessarily result in a unique solution raises uncertainty in the refined site positions (see SI for more details). Therefore, the disagreement is likely partially a result of crystallographic limitations rather than simulation



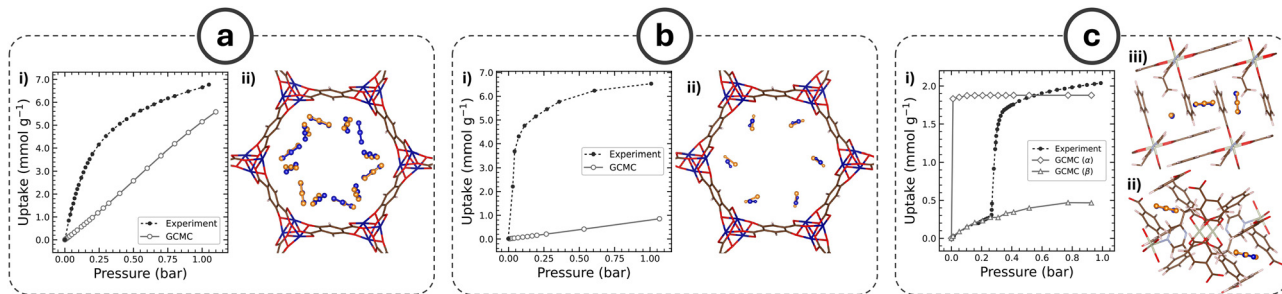


Fig. 2 Comparisons of binding sites and adsorption isotherms between GCMC and experiment for (a) MOF-74(Co)@CO₂ (MAC 26), (b) MOF-74(Co)@NO (MAC 27), and (c) [Rh₂(bza)₄(2-epy)₂]_n@CO₂ (MACs 1–2). The simulated (blue) and experimental (orange) binding sites correspond to conditions specified in Table 1. The atoms of NO with larger radii in (b) correspond to oxygen. The isotherms correspond to temperatures of (a), (b) 304 K, and (c) 195 K. Structures in (c) correspond to the (ii) α and (iii) β phases.

failure alone. The benzoate pyrazines in this work still exhibit low RMSDs despite adsorption-induced transitions, likely because their phase changes occur over a narrow pressure window with limited local flexibility (consistent with the isotherms). We also reiterate that we modelled the phase corresponding to the *in situ* XRD conditions used to determine the experimental sites. MAF-23 shows analogous flexibility, though at a local rather than global scale. For MAF-23@CO₂ (35) (Fig. S34), the secondary site is notably worse, consistent with the original report that CO₂ binding between chelating triazoles induces a small conformational change, so while the low-pressure regime is reproduced, rigid modelling likely underestimates the saturation uptake.

Another exception with qualitative disagreement in the binding sites arises for MOF-74@NO, where unlike the previous examples there is no notable flexibility, but there is a considerable degree of chemisorption. In MOF-74(Co)@NO (27) and MOF-74(Ni)@NO (31), the simulated primary ABS has NO bound to the OMS *via* O instead of N as observed experimentally. This is because the interaction is expected to be chemisorptive to a large degree, and the generic classical force field is unable to treat such an interaction properly. This is also reflected in the simulated isotherm, which severely underestimates uptake as shown in the MOF-74(Co)@NO isotherm (Fig. 2b(i)). However, the centre of mass of the ABS is nevertheless correctly predicted. We note the NO bond distance from crystallography is unusually long (1.43 Å), whereas the value used in the GCMC simulation is 1.15 Å (much closer to the 1.18 Å length obtained from a full geometry optimization of MOF-74(Co)@NO at the DFT level). To separate chemisorption effects from NO-specific complexity, we also examined a secondary physisorptive NO ABS in MOF-74(Ni)@NO where the OMSs are capped with H₂O (Fig. S13, MAC 11). There is still some disagreement between experimental and simulated ABSs (with experimental disorder noted in the nitrogen position of NO),³⁰ but the qualitative binding motif is recovered: a dipole “chain” from H₂O(δ^+) \rightarrow O_{NO}(δ^-) \rightarrow N_{NO}(δ^+) \rightarrow MOF carboxylate (δ^-) (Fig. S2). Overall, the large errors for MOF-74@NO likely reflect both OMS limitations and the challenges of modelling a reactive, open-shell adsorbate with a classical force field. Despite generally good agreement, an important question

is whether other force fields predict the same ABSs. In this work, sensitivity of the ABSs to the force fields used to model adsorbate interactions were not investigated, since the ABSs were found to be largely insensitive to the choice of force field for the framework atoms. However, we note that other available or more specialized adsorbate force fields may exhibit higher accuracy for modelling certain ABSs. Most MOF screening studies model sterics/dispersion with UFF Lennard-Jones potentials and electrostatics with ESP-fitted charges (*e.g.*, REPEAT,¹⁸ DDEC¹⁹) or charge equilibration (MEPO-QEq¹⁶). Excluding MOF-74(Zn) and MOF-74(Fe), where metal parameters differ drastically (DREIDING RMSD/atom = 3.4 and 2.6 Å), UFF and DREIDING force fields give the same mean RMSD (0.56 Å). Empirical charges such as QEq often give qualitatively different results with the wrong number of sites, but MEPO-ML¹⁷ (trained to reproduce ESP-fitted charges) provides a low cost alternative to DFT-derived charges with comparable accuracy (RMSD/atom = 0.63 Å). We therefore recommend UFF with DFT-quality charges for reliable ABS prediction. Across diverse MOFs and adsorbates, direct comparison to crystallography shows that classical GCMC reliably predicts physisorptive ABSs when the correct framework phase is used. Notably, predicted ABSs are accurate even when isotherms are poorly reproduced because they depend more on relative than absolute energetics. Accuracy diminishes with chemisorption, strong flexibility, and substantial experimental disorder. Adsorbate complexity also plays an important role, which can arise from, among other factors, strong multipole moments and open-shell character. An important aspect is highly polarizable adsorbates (*e.g.*, water), since polarizability is not explicitly accounted for in most force fields. We expect the atomistic simulation approach validated in this work to extend well to porous materials other than MOFs, so long as the binding is primarily physisorptive, the force field of the adsorbate is reliable for modelling adsorption, and the porous material does not exhibit a large degree of flexibility (*e.g.*, zeolites and COFs). In materials where electrostatic interactions are expected to dominate over dispersion, such as zeolites, DFT-quality charges are expected to be increasingly important. In the case of COFs, better agreement may be expected in some cases due to reduced modelling complexity in the absence of



inorganic units, but care should be taken to ensure adsorbate binding does not induce phase changes (e.g., changes in stacking behaviour in 2D COFs). Outside these cases, routine simulations offer a practical way to resolve ABSs that are often inaccessible experimentally, providing a benchmark for future methods and a tool for diagnosing experiment–simulation discrepancies in MOF adsorption. The dataset curated in this work will also serve as a useful benchmark for future studies that aim to move beyond the approximations used in conventional atomistic simulations to obtain more accurate adsorption properties and ABSs.

Author contributions

Conceptualization, writing – review & editing: JB, OM, MG, TW; data curation: JB, OM, SW, MG; formal analysis, investigation, validation, methodology: JB, OM; writing – original draft preparation: JB, OM, TW; funding acquisition, resources, supervision: TW.

Conflicts of interest

There are no conflicts to declare.

Data availability

The CIF files for each MOF in the dataset, along with their corresponding atomic charges, are available on Zenodo at <https://zenodo.org/records/17991796>. The binding site outputs generated using our in-house GALP code, together with the folded adsorption density profiles, are also provided for each MOF and for each force field/charge combination: UFF/REPEAT, UFF/DDEC6, UFF/MEPO-ML, DREIDING/REPEAT, DREIDING/DDEC6, and DREIDING/MEPO-ML. These datasets can be accessed on Zenodo at <https://zenodo.org/records/17993963>.

Supplementary information: details of experimental dataset preparation, computational details, force field sensitivity analysis, visualized binding site comparisons, and isotherm comparisons. See DOI: <https://doi.org/10.1039/d6ma00185h>.

Acknowledgements

Authors thank the Natural Sciences and Engineering Research Council of Canada (DISCOVERY Grant), the University of Ottawa, MITACS (Accelerate) and TotalEnergies for financial support and the Digital Research Alliance of Canada for computing resources.

References

- J.-B. Lin, T. T. T. Nguyen, R. Vaidhyanathan, J. Burner, J. M. Taylor, H. Durekova, F. Akhtar, R. K. Mah, O. Ghaffari-Nik, S. Marx, N. Fylstra, S. S. Iremonger, K. W. Dawson, P. Sarkar, P. Hovington, A. Rajendran, T. K. Woo and G. K. H. Shimizu, *Science*, 2021, **374**, 1464–1469.
- G. Ozin, *CALF-20: A carbon capture success story*, 2022, <https://www.advancedsciencenews.com/calf-20-a-carbon-capture-success-story/>.
- C. Bettenhausen, *C&EN Global Enterp.*, 2023, **101**, 13.
- M. Jacoby, *C&EN Global Enterp.*, 2016, **94**, 32.
- P. G. Boyd, A. Chidambaram, E. García-Díez, C. P. Ireland, T. D. Daff, R. Bounds, A. Gładysiak, P. Schouwink, S. M. Moosavi, M. M. Maroto-Valer, J. A. Reimer, J. A. R. Navarro, T. K. Woo, S. Garcia, K. C. Stylianou and B. Smit, *Nature*, 2019, **576**, 253–256.
- Y. Chen, W. Lu, M. Schröder and S. Yang, *Acc. Chem. Res.*, 2023, **56**, 2569–2581.
- P. Z. Moghadam, A. Li, S. B. Wiggin, A. Tao, A. G. P. Maloney, P. A. Wood, S. C. Ward and D. Fairen-Jimenez, *Chem. Mater.*, 2017, **29**, 2618–2625.
- A. Li, R. Bueno-Perez, S. Wiggin and D. Fairen-Jimenez, *CrystEngComm*, 2020, **22**, 7152–7161.
- T. L. Easun, F. Moreau, Y. Yan, S. Yang and M. Schröder, *Chem. Soc. Rev.*, 2017, **46**, 239–274.
- Z. Han, K.-H. Yu, K.-Y. Wang and H.-C. Zhou, *Energy Fuels*, 2025, **39**, 6151–6163.
- B. E. G. Lucier, S. Chen and Y. Huang, *Acc. Chem. Res.*, 2018, **51**, 319–330.
- V. Martins, B. E. Lucier, Z. Liu, H. Liang, A. Zheng, V. V. Terskikh, W. Zhang, B. E. Desveaux and Y. Huang, *Inorg. Chem.*, 2023, **62**, 11152–11167.
- Y. A. Ran, S. Sharma, S. R. G. Balestra, Z. Li, S. Calero, T. J. H. Vlught, R. Q. Snurr and D. Dubbeldam, *J. Chem. Phys.*, 2024, **161**, 114106.
- C. Cleeton, F. L. d Oliveira, R. F. Â. Neumann, A. H. Â. Farmahini, B. Luan, M. Steiner and L. Sarkisov, *Energy Environ. Sci.*, 2023, **16**, 3899–3918.
- A. K. Rappe, C. J. Casewit, K. S. Colwell, W. A. I. Goddard and W. M. Skiff, *J. Am. Chem. Soc.*, 1992, **114**, 10024–10035.
- E. S. Kadantsev, P. G. Boyd, T. D. Daff and T. K. Woo, *J. Phys. Chem. Lett.*, 2013, **4**, 3056–3061.
- J. Luo, O. B. Said, P. Xie, M. Gibaldi, J. Burner, C. Pereira and T. K. Woo, *npj Comput. Mater.*, 2024, **10**, 224.
- C. Campaña, B. Mussard and T. K. Woo, *J. Chem. Theory Comput.*, 2009, **5**, 2866–2878.
- T. A. Manz and D. S. Sholl, *J. Chem. Theory Comput.*, 2010, **6**, 2455–2468.
- C. McCready, K. Sladekova, S. Conroy, J. R. B. Gomes, A. J. Fletcher and M. Jorge, *J. Chem. Theory Comput.*, 2024, **20**, 4869–4884.
- Z. Yu, D. M. Anstine, S. E. Boulfelfel, C. Gu, C. M. Colina and D. S. Sholl, *ACS Appl. Mater. Interfaces*, 2021, **13**, 61305–61315.
- R. Goeminne and V. Van Speybroeck, *J. Am. Chem. Soc.*, 2025, **147**, 3615–3630.
- S. Takamizawa, E.-I. Nataka, T. Akatsuka, R. Miyake, Y. Kakizaki, H. Takeuchi, G. Maruta and S. Takeda, *J. Am. Chem. Soc.*, 2010, **132**, 3783–3792.
- J. Drweska, F. Formalik, K. Roztock, R. Q. Snurr, L. J. Barbour and A. M. Janiak, *Inorg. Chem.*, 2024, **63**, 19277–19286.



- 25 S. Bette, A. Sleptsova, B. V. Lotsch, R. E. Dinnebier, S. Marx, M. Loloie, A. A. Adeleke, N. Masoumifard and R. Vaidhyanathan, *J. Am. Chem. Soc.*, 2025, **147**, 25662–25671.
- 26 D. G. Samsonenko, H. Kim, Y. Sun, G.-H. Kim, H.-S. Lee and K. Kim, *Chem. – Asian J.*, 2007, **2**, 484–488.
- 27 R. Vaidhyanathan, S. S. Iremonger, G. K. H. Shimizu, P. G. Boyd, S. Alavi and T. K. Woo, *Science*, 2010, **330**, 650–653.
- 28 S. R. Miller, P. A. Wright, T. Devic, C. Serre, G. Férey, P. L. Llewellyn, R. Denoyel, L. Gaberova and Y. Filinchuk, *Langmuir*, 2009, **25**, 3618–3626.
- 29 O. T. Qazvini, R. Babarao and S. G. Telfer, *Nat. Commun.*, 2021, **12**, 197.
- 30 R. M. Main, R. Ettlenger, T. K. Tajnšek, D. A. Brako-Amofo, M. G. Stanzione, M. J. Duncan, P. Ettlenger, G. B. Lawrence, M. R. Warren, C. J. Heard and R. E. Morris, *J. Am. Chem. Soc.*, 2025, **147**, 31260–31269.
- 31 D. Banerjee, C. M. Simon, A. M. Plonka, R. K. Motkuri, J. Liu, X. Chen, B. Smit, J. B. Parise, M. Haranczyk and P. K. Thallapally, *Nat. Commun.*, 2016, **7**, 11831.
- 32 S. Takamizawa, E.-i Nakata, T. Saito and K. Kojima, *CrytEngComm*, 2003, **5**, 411–413.
- 33 S. Takamizawa, E.-i Nakata, H. Yokoyama, K. Mochizuki and W. Mori, *Angew. Chem., Int. Ed.*, 2003, **42**, 4331–4334.
- 34 S. Takamizawa, E.-i Nakata and T. Saito, *Inorg. Chem. Commun.*, 2004, **7**, 1–3.
- 35 S. Takamizawa, K. Kojima and T. Akatsuka, *Inorg. Chem.*, 2006, **45**, 4580–4582.
- 36 S. Couck, E. Gobechiya, C. E. A. Kirschhock, P. Serra-Crespo, J. Juan-Alcañiz, A. Martinez Joaristi, E. Stavitski, J. Gascon, F. Kapteijn, G. V. Baron and J. F. M. Denayer, *ChemSusChem*, 2012, **5**, 740–750.
- 37 R. Matsuda, R. Kitaura, S. Kitagawa, Y. Kubota, R. V. Belosludov, T. C. Kobayashi, H. Sakamoto, T. Chiba, M. Takata, Y. Kawazoe and Y. Mita, *Nature*, 2005, **436**, 238–241.
- 38 M. Chen, S. Chen, W. Chen, B. E. G. Lucier, Y. Zhang, A. Zheng and Y. Huang, *Chem. Mater.*, 2018, **30**, 3613–3617.
- 39 W. L. Queen, M. R. Hudson, E. D. Bloch, J. A. Mason, M. I. Gonzalez, J. S. Lee, D. Gygi, J. D. Howe, K. Lee, T. A. Darwish, M. James, V. K. Peterson, S. J. Teat, B. Smit, J. B. Neaton, J. R. Long and C. M. Brown, *Chem. Sci.*, 2014, **5**, 4569–4581.
- 40 A. C. McKinlay, B. Xiao, D. S. Wragg, P. S. Wheatley, I. L. Megson and R. E. Morris, *J. Am. Chem. Soc.*, 2008, **130**, 10440–10444.
- 41 T. K. Maji, G. Mostafa, R. Matsuda and S. Kitagawa, *J. Am. Chem. Soc.*, 2005, **127**, 17152–17153.
- 42 J.-P. Zhang and X.-M. Chen, *J. Am. Chem. Soc.*, 2009, **131**, 5516–5521.
- 43 P.-Q. Liao, D.-D. Zhou, A.-X. Zhu, L. Jiang, R.-B. Lin, J.-P. Zhang and X.-M. Chen, *J. Am. Chem. Soc.*, 2012, **134**, 17380–17383.
- 44 S. N. Rao, M. S. Head, A. Kulkarni and J. M. LaLonde, *J. Chem. Inf. Model.*, 2007, **47**, 2159–2171.

